Scripta Materialia 232 (2023) 115496

Contents lists available at ScienceDirect

Scripta Materialia

journal homepage: www.journals.elsevier.com/scripta-materialia

Computational thermodynamics and kinetics-guided re-engineering of a high-performance tool steel

Tao Zhou [a,*], Gabriel Spartacus [a], Alexander Dahlström [a], R. Prasath Babu [a], Anton Davydok [b], Peter Hedström [a]

[a] Department of Materials Science and Engineering, KTH Royal Institute of Technology, Stockholm, SE 100 44, Sweden
[b] Helmholtz-Zentrum Hereon, Max-Planck-Straße 1, Geesthacht 21502, Germany

ARTICLE INFO

Keywords:
Alloy development
Computational thermodynamics
Precipitation kinetics
Advanced characterization
Tool steels

ABSTRACT

Targeting to obtain fine dispersions of nanoscale precipitates to enhance the mechanical properties of a high-performance tool steel, re-engineering of the alloy composition and heat treatment was guided by computational thermodynamics and kinetics. A prototype alloy was prepared using the designed chemistry and heat treatment. Thereafter, advanced microstructural characterization and mechanical testing confirmed the successful design to reach a high number density of (V, Mo)C precipitates with an average diameter of about 5 nm in the peak-hardened condition, after tempering the martensite at 600 °C for 2 h.

The development of high-performance tool steels is important in order to withstand the harsh service conditions of machine parts. Conventional tool steels are characterized by a medium/high-carbon content and carbide-forming elements including Cr, Mo and V to stimulate precipitation of carbides and ensure high strength and hardness. There are, however, some limitations for this kind of alloying: i) a high carbon content significantly impairs the toughness and weldability of tool steels; ii) coarse carbides including M_3C, M_6C, $M_{23}C_6$, *etc*. are formed during the final heat treatment [1,2], and they have limited contributions to strength/hardness and even deteriorate the toughness of the tool steel; iii) the formed carbides have high coarsening rate, with low thermal softening resistance, which reduces the strength of the material and the lifetime of machine parts at elevated service temperatures. To mitigate these problems that limit the performance of tool steels, in this work we aim to re-engineer a high-performance tool steel using the guidance from computational thermodynamics and kinetics. The new alloy is expected to improve and balance a combination of important properties such as toughness, thermal stability and weldability using a lean metallurgical concept, but still maintaining comparable strength/hardness as the conventional tool steel in *Refs*. [1,2]. Obtaining the more balanced properties will depend on the successful optimization of precipitates with fine dispersions of nanoscale carbides (*e.g.*, MC and M_2C with M representing mainly V and Mo), whilst limiting the formation of coarser carbide populations [3]. The fine dispersion of MC or/and M_2C nanoscale carbides are expected to have the following merits: i) higher contribution to strength, hardness, and wear resistance at ambient and elevated temperatures [4]; ii) high stability of the materials during service at elevated temperature due to the lower growth and coarsening rates of the precipitates [5,6]; iii) potential hydrogen trapping sites, enhancing hydrogen embrittlement resistance of the material [7]. Some guiding principles for the new alloy are that coarse carbide particles should not be present in the final product's microstructure, *i.e.* they should not be thermodynamically stable; and moreover, the ratio of C/(V+Mo) should be maintained close to unity to not only facilitate nanoscale precipitation (strengthening the alloy) but also to decrease the C content in solid solution in the final product's microstructure (increasing the toughness). Therefore, firstly computational thermodynamics and kinetics were carried out to determine the re-engineered alloying and heat treatment parameters, targeting the desirable fine precipitation types MC or/and M_2C. Thereafter, a prototype material was prepared based on the aforementioned materials design philosophy, and characterization using advanced experimental tools were carried out for validation, focusing on the precipitation.

The computational thermodynamics were performed using the Thermo-Calc software [8] with TCFE10 database. The precipitation kinetics were simulated using Langer–Schwartz–Kampmann–Wagner-type modeling [9] implemented in the precipitation simulation module of the Thermo-Calc software coupled with TCFE10 and MOBFE5 databases. The simulation results were subsequently used to guide the determination of alloy chemistry and heat treatment parameters. The scanning

* Corresponding author.
E-mail address: taozhou@kth.se (T. Zhou).

https://doi.org/10.1016/j.scriptamat.2023.115496
Received 17 March 2023; Accepted 13 April 2023
Available online 19 April 2023

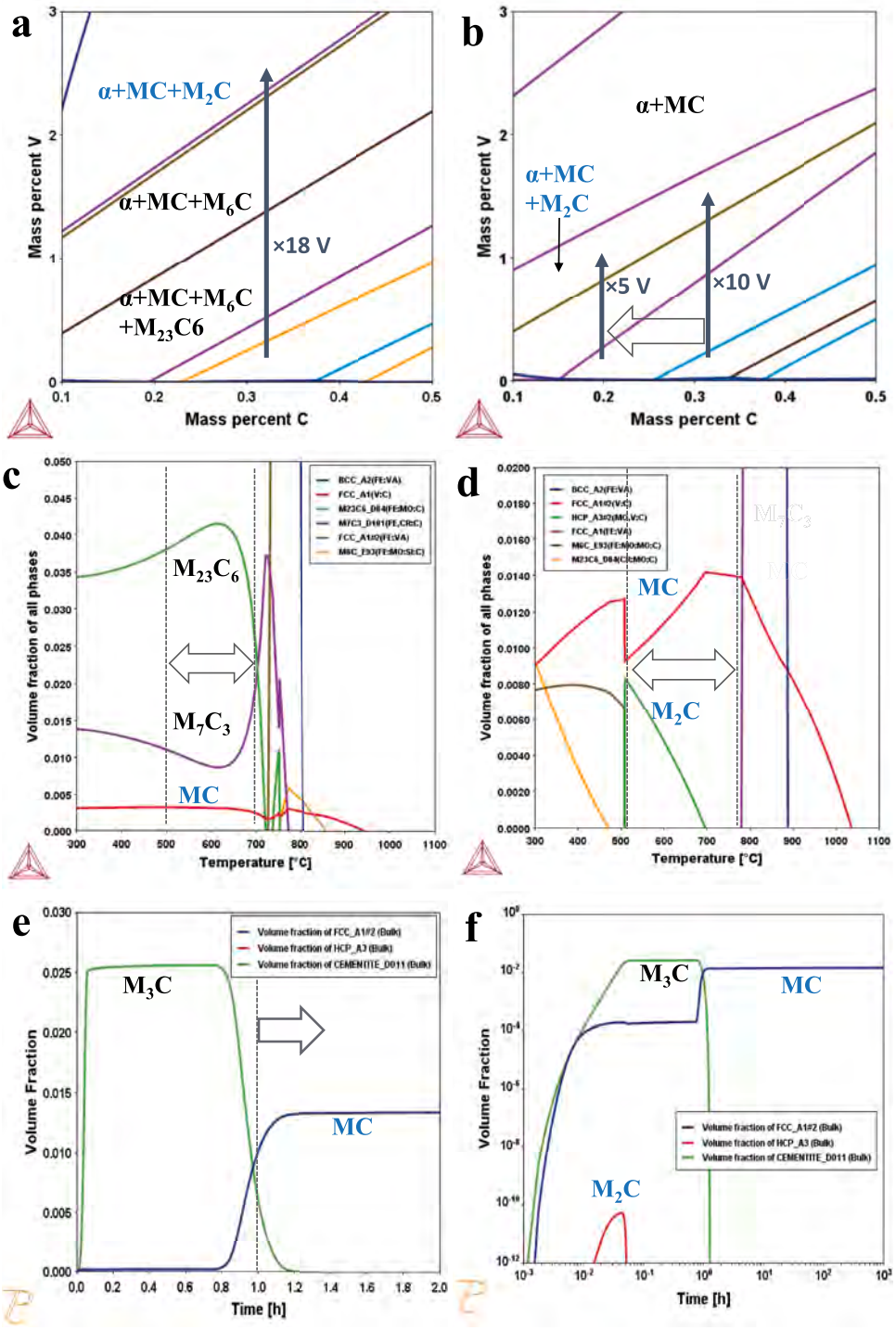

Fig. 1. Computational thermodynamics and kinetics for precipitation design: a. isothermal phase diagram at 550 °C with variations in C and V in a previously studied reference steel with chemical composition of 0.32C–1.1Si–0.8Mn–1.4Cr–0.8Mo–0.14V–0.7Ni; b. isothermal phase diagram at 650 °C with variations in C and V after reducing the Si content from 1.1 wt% to 0.3 wt% of the reference steel; c. property diagram of the reference steel; d. the property diagram of the new steel; e. precipitation kinetics modeling of the new steel at 600 °C for 2 h; f. precipitation kinetics modeling of the new steel at 600 °C for 1000 h with logarithmic scale of y-axis.

electron microscopy (SEM) imaging and electron backscatter diffraction (EBSD) analysis were carried out using a JEOL-7800F SEM equipped with a Bruker Quantax EBSD system. The scanning transmission electron microscopy combined with energy dispersive spectroscopy (STEM-EDS) was done using a FEI Titan Themis 200 TEM equipped with a probe spherical-aberration corrector and a SuperX EDS. The atom probe tomography (APT) was conducted using a LEAP 3000XHR in laser pulse mode with a pulse rate 200 kHz, laser pulse energy 0.3 nJ, evaporation rate 0.5%, and sample temperature 65 K. Samples were prepared using the two-stage electropolishing method. The data reconstruction and analysis were made using the software IVAS 3.8.0. X-ray diffraction (XRD) patterns were measured at the nanofocus endstation of the P03 beamline, PETRA III. The x-ray energy was set to 17 keV, with a beam size of 1.5 × 1.5 μm^2. In order to increase the statistics, 100 measurements were performed over an area of 90 × 90 μm^2 on each sample of around 30 μm thickness, following a 10 × 10 equally spaced square measurement pattern, and then these 100 measurements were averaged. This approach also allows to confirm whether or not the detected phases are homogeneously distributed in the sample volume. The 2D diffraction patterns were collected on a Dectris Eiger 9 M detector at a sample-to-detector distance of ~0.2 m, calibration was performed using a LaB_6 reference sample and azimuthal integration was carried out using pyFAI [10].

The findings in our previous work [1] suggest that tuning the V

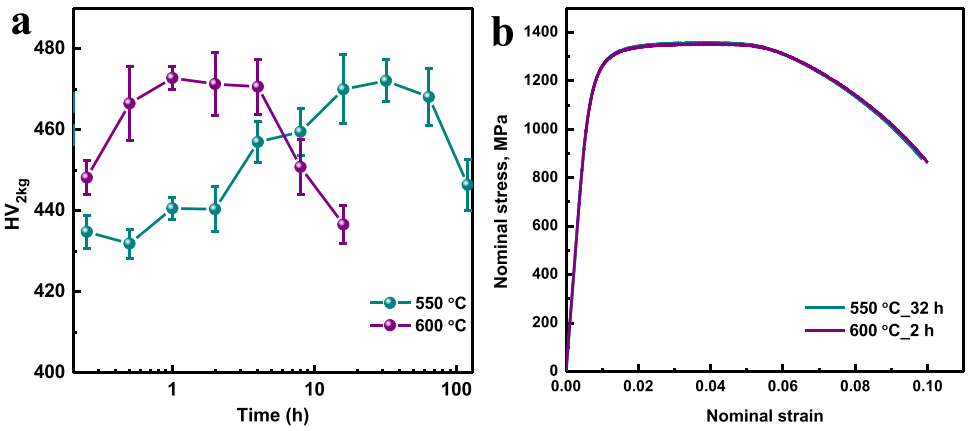

Fig. 2. Mechanical properties of the prototype steel: a. hardness variations under different solid solution and tempering treatment conditions; b. tensile stress-strain curves of the peak-hardened conditions found in figure a.

content, instead of Cr and Mo contents is effective to avoid the coarse precipitation phases, but the 550 °C isothermal phase diagram of the reference steel (see Fig. 1a) suggests that at least 18 times more V is needed (> 2wt%) as compared to the reference steel in order to obtain an equilibria of bcc-Fe matrix, and MC and M_2C carbides. This large increase of V is less attractive from a commercial perspective considering the high alloying cost. Instead, through adjusting the content of other alloying elements and the temperature, we can reach the desired phase region with fine precipitates at a lower V content, as shown in Fig. 1b. In this figure it is shown that around 10 times higher V content is needed after reducing the Si content and increasing the temperature. In addition, it can be noted that if the C content could be reduced, the required increase in V content would be much less. This minor alloying cost increase, coming from the increase in V content, could be industrially acceptable if better or more balanced properties can be achieved. The property diagram of the new alloy shown in Fig. 1d, in comparison to Fig. 1c for the reference alloy, suggests that the stable precipitation phases at a wide temperature range of around 500–780 °C are merely MC and M_2C, which provides a large process window for the tempering treatment. Precipitation kinetics modeling shown in Fig. 1e and f predicts that the thermodynamically metastable M_3C quickly forms after tempering at 600 °C, which dissolves after ~1 h at the benefit of MC precipitation, which then becomes the dominant precipitate phase. A negligible amount of M_2C could form at the early stage of tempering, but it is kinetically metastable and quickly dissolves. Moreover, a previous study [11] suggests that the V/Mo ratio should be quite low to precipitate M_2C in similar alloy systems; therefore, we do not expect to have such precipitates with a relatively high V/Mo ratio (around 1.0) in the new steel. Guided by the above calculations and the previous knowledge on the similar alloys, a prototype material with a chemical composition of 0.17C–0.5Si–0.8Mn–1.4Cr–0.8Mo–0.85V–0.7Ni (wt%) was manufactured as a 30 kg round ingot with a diameter ranging from 70 to 100 mm by vacuum induction melting, then forged to a slab with a cross-section of around 30 × 30 mm^2 at 1200 °C, before hot-rolling to a plate with thickness ~4 mm and air cooled to room temperature. Thereafter, the material was solution treated at 1100 °C (that is ~50 °C higher than the calculated dissolution temperature of MC in Fig. 1d) for 1 h, water quenching, before tempering at 550 °C and 600 °C for various durations. The Vickers hardness tests were carried out on the heat treated samples under 2 kg load and the tensile tests were performed for peak-hardened sample conditions at 550 °C and 600 °C.

The new steel shows a clear secondary hardening effect after tempering (see Fig. 2a), in comparison to the reference steel for which no obvious secondary hardening effect was observed [2]. The peak hardening conditions are at 550 °C found after 32 h and at 600 °C found after 2 h, and both peak hardened conditions achieve a hardness of about 475 HV. The hardness results also indicate that the precipitate phase is quite thermally stable, *i.e.* its coarsening can only occur rapidly when the temperature is above around 550 °C. The stress-strain curves of the two peak-hardened conditions are almost identical (see Fig. 2b), with yield strength of ~1270 MPa, ultimate tensile strength of ~1365 MPa, and total elongation of ~10%. The mechanical properties of the

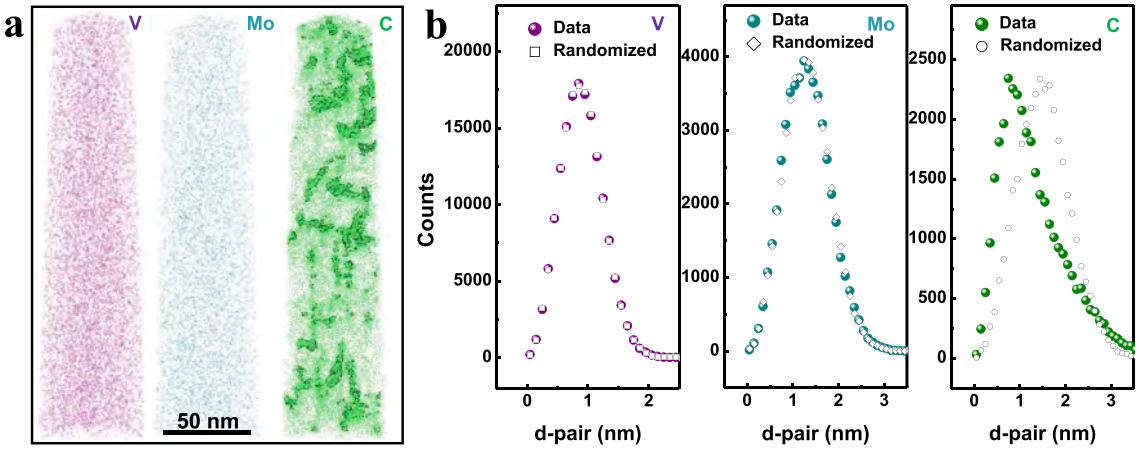

Fig. 3. a. 3D atomic distribution of elements V, Mo and C (together with 1 at%C isosurface) in the as-quenched sample; b. the corresponding nearest neighbor distribution of V–V, Mo–Mo, and C–C pairs.

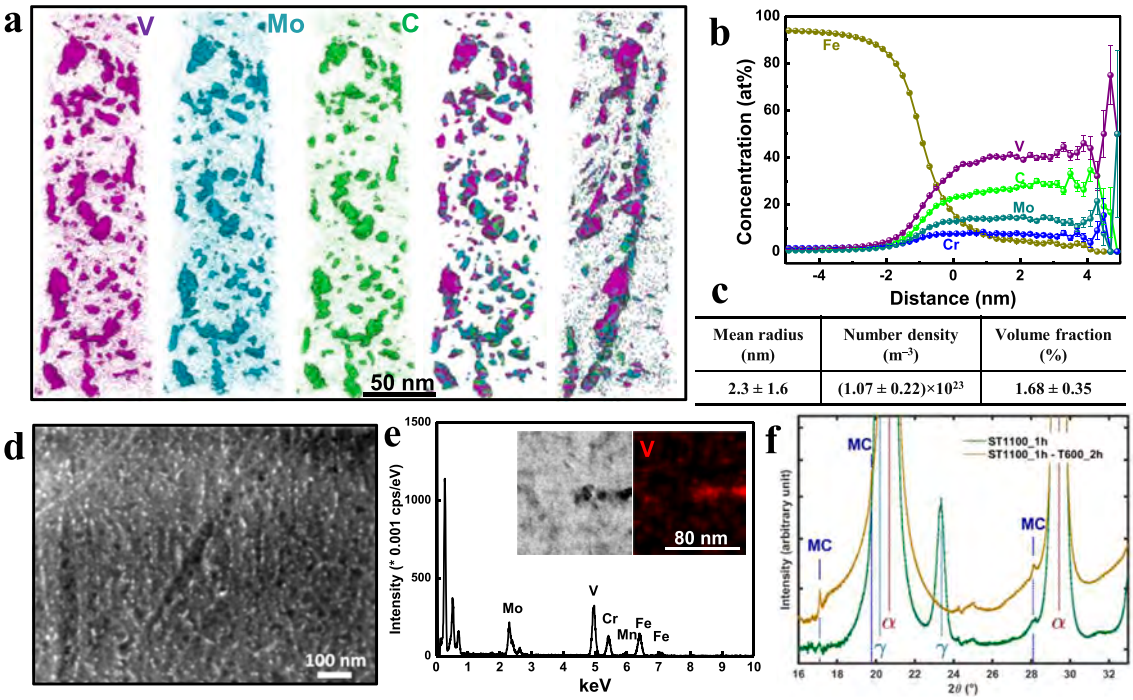

Fig. 4. a. APT reconstruction of the V- and Mo- rich carbides in the 600 °C-2 h sample, showing, in the sequence, V atoms with 20 at%V isosurface, Mo atoms with 10 at%Mo isosurface, C atoms with 20 at%C isosurface, 20 at%V isosurface + 10 at%Mo isosurface + 20 at%C isosurface, and the location of the carbides on martensitic boundaries after rotating the volume; b. the average atomic concentrations within the precipitates shown in image a using the proxigram method; c. the quantification of the carbides shown in the image following the method detailed in ref. [9]; d. a SEM image showing the distribution of carbides in the martensite matrix; e. STEM-EDS analysis of the chemical composition of the carbides, with bright-field image and EDS mapping of V shown as insets; f. Synchrotron XRD patterns after background subtraction showing the phases present in the as-quenched and peak-hardened samples.

prototype material are comparable to those of the commercial reference steel [2], even though the contents of C and Si are significantly reduced (~50% each) and it is well-known that both C and Si have a significant effect on hardness/strength of martensite. The microstructure characterization was performed to validate the computational thermodynamics and kinetics as shown in Fig. 1. The as-quenched sample has a typical lath martensite microstructure. The V and Mo atoms are uniformly distributed in the volume, but carbon segregation occurs due to autotempering of martensite during the quenching process, see Fig. 3a. The nearest neighbor distribution analysis of the atomic pairs (see Fig. 3b) further confirms that no obvious clustering of V or Mo is present in the as-quenched sample. In contrast, the peak-hardened sample has a high number of V- and Mo-rich carbides, see APT results in Fig. 4a. The APT images (see the last image in Fig. 4a) suggest that most of the precipitates are located in two planes, which are probably the lath boundaries. This is in good agreement with the SEM image (see Fig. 4d) where the precipitates are also aligned. The carbides are V-rich, but with a high content of Mo, together with potentially a small amount of Fe and Cr, as indicated by the APT proxigram analysis (Fig. 4b) and the STEM-EDS analysis (Fig. 4e). These carbides are of nanometric size and approximately 5 nm in diameter in the peak-hardened condition. The carbides have a high number density, in the order of 10^{23} m^{-3} (Fig. 4c), which is comparable to that of Cu precipitate [12] and intermetallic precipitate phases [13] in maraging steels. In addition, synchrotron XRD was performed to confirm the structure of the observed V- and Mo-rich carbides and to have better statistical analysis of the precipitate phases. The MC phase with a face-centered cubic structure (FCC) corresponding to (V, Mo)C carbide was identified (Fig. 4f). The unit cell of the identified (V, Mo)C phase has a lattice parameter of 4.247 Å, displaying a higher cell parameter than that of VC (4.182 Å [14]), which likely results from the presence of high content of Mo atoms in the precipitates. Tiny peaks are also observed on the similar peak positions of the (V, Mo)C phase for the as-quenched sample. This may come from the presence of a minor amount of Ti(C, N) phase (lattice parameter in the range of 4.250–4.324 Å [15]) in the steel. The XRD measurements suggest that MC carbides are fairly homogeneously dispersed over the scanned volume (90 × 90 × 30 μm^3). Retained austenite was also identified in the as-quenched sample, but it completely decomposes in the peak-hardened condition.

In summary, this work has employed computational thermodynamics and kinetics for the re-engineering of a high-performance tool steel to replace the typical coarser carbides with fine carbide precipitates of the MC or M_2C type. A prototype steel was prepared and heat treated according to the computational design. Microstructural characterization and mechanical testing of the prototype material were thereafter performed to study the outcome of the computational design. The results show that a high number density (~10^{23} m^{-3}) of (V, Mo)C precipitates with mean size of about 5 nm form, without the presence of the coarse carbides existing in the reference steel. These findings illustrate the significant potential of computational thermodynamics and kinetics together with advanced characterization for re-engineering steel alloys and their heat treatments to optimize performance.

Declaration of Competing Interest

The authors declare that they have no known competing financial interests or personal relationships that could have appeared to influence the work reported in this paper.

Funding

This research was funded by the Carl Tryggers Foundation (CTS19: 136), and the Competence Center Hero-m 2 Innovation (financed by VINNOVA, Swedish Industry, and KTH). The authors are grateful to PETRA III high-energy synchrotron source, DESY, Germany for providing synchrotron radiation facilities at the beamline P03. The

authors gratefully acknowledge the APT support provided by Mattias Thuvander at Chalmers Materials Analysis Laboratory (CMAL), and by the Hultgren laboratory at KTH. The authors are also grateful to Ziyong Hou at Chongqing University and Maokun Bai at Northeastern University (111 project, Grant No. B16009) for preparing the prototype material.

References

[1] T. Zhou, R.P. Babu, Z. Hou, J. Odqvist, P. Hedström, Precipitation of multiple carbides in martensitic CrMoV steels-experimental analysis and exploration of alloying strategy through thermodynamic calculations, Materialia 9 (2020), 100630.
[2] T. Zhou, J. Lu, P. Hedström, Mechanical behavior of fresh and tempered martensite in a CrMoV-alloyed steel explained by microstructural evolution and strength modeling, Metall. Mater. Trans. A 50 (2020) 5077–5087.
[3] H.M. Lee, S.M. Allen, Coarsening resistance of M2C carbides in secondary hardening steels: part III. Comparison of theory and experiment, Metall. Trans. A 22 (1991) 2877–2888.
[4] J.S. Wang, M.D. Mulholland, G.B. Olson, D.N. Seidman, Prediction of the yield strength of a secondary-hardening steel, Acta Mater. 61 (2013) 4939–4952.
[5] H.M. Lee, S.M. Allen, M. Grujicic, Coarsening resistance of M_2C carbides in secondary hardening steels: part I. Theoretical model for multicomponent coarsening kinetics, Metall. Trans. A 22 (1991) 2863–2868.
[6] H.M. Lee, S.M. Allen, M. Grujicic, Coarsening resistance of M_2C carbides in secondary hardening steels: part II. Alloy design aided by a thermochemical database, Metall. Trans. A 22 (1991) 2869–2876.
[7] B. Zhang, J. Su, M. Wang, Z. Liu, Z. Yang, M. Militzer, H. Chen, Atomistic insight into hydrogen trapping at MC/BCC-Fe phase boundaries: the role of local atomic environment, Acta Mater. 208 (2021), 116744.
[8] J.O. Andersson, T. Helander, L. Höglund, P. Shi, B. Sundman, Thermo-Calc & DICTRA, computational tools for materials science, Calphad 26 (2002) 273–312.
[9] Z. Sheng, M.B. Rolland, T. Zhou, J. Odqvist, P. Hedström, Langer–Schwartz–Kampmann–Wagner precipitation simulations: assessment of models and materials design application for Cu precipitation in PH stainless steels, J. Mater. Sci. 56 (2021) 2650–2671.
[10] G. Ashiotis, A. Deschildre, Z. Nawaz, J.P. Wright, D. Karkoulis, F.E. Picca, J. Kieffer, The fast azimuthal integration Python library: pyFAI, J. Appl. Crystallogr. 48 (2015) 510–519.
[11] E. Claesson, H. Magnusson, J. Kohlbrecher, M. Thuvander, F. Lindberg, M. Andersson, P. Hedström, carbide precipitation during processing of two low-alloyed martensitic tool steels with 0.11 and 0.17V/Mo ratios studied by neutron scattering, electron microscopy and atom probe, Metals (Basel) 12 (2022) 758.
[12] T. Zhou, B. Neding, S. Lin, J.C. Tseng, P. Hedström, Cu precipitation-mediated formation of reverted austenite during ageing of a 15–5 PH stainless steel, Scr. Mater. 202 (2021), 114007.
[13] S. Jiang, H. Wang, Y. Wu, X. Liu, H. Chen, M. Yao, B. Gault, D. Ponge, D. Raabe, A. Hirata, M. Chen, Y. Wang, Z. Lu, Ultrastrong steel via minimal lattice misfit and high-density nanoprecipitation, Nature 544 (2017) 460–464.
[14] R.W.G. Wyckoff, R.W. Wyckoff, Crystal Structures, Interscience publishers, New York, 1963.
[15] Y. Tian, H. Yu, T. Zhou, K. Wang, Z. Zhu, Revealing morphology rules of MX precipitates in Ti-V-Nb multi-microalloyed steels, Mater. Charact. 188 (2022), 111919.